Chemical bonding and transport properties in clathrates-I with Cu-Zn-P frameworks

Juli-Anna Dolyniuk,[a] Jian Wang,[b,c] Maxwell Marple,[d] Sabyasachi Sen,[d] Yongqiang Cheng,[e] A. J. Ramirez-Cuesta,[e] Kirill Kovnir[b,c,*]

[a] *Department of Chemistry, University of California, Davis, Davis, California, 95616, USA*

[b] *Department of Chemistry, Iowa State University, Ames, Iowa 50011, USA*

[c] *Ames Laboratory, U.S. Department of Energy, Ames, Iowa 50011, USA*

[d] *Department of Materials Science and Engineering, University of California, Davis, Davis, California, 95616, USA*

[e] *Chemical and Engineering Materials Division, Oak Ridge National Laboratory, Oak Ridge, Tennessee, 37830, USA*

Abstract

Quaternary clathrate-I phases with an overall composition of $Ba_8M_{16+y}P_{30-y}$ (M = Cu,Zn) exhibit complex structural chemistry. Characterization of the electronic structures and chemical bonding using quantum-chemical calculations and ^{31}P solid state NMR spectroscopy demonstrated that the Cu-Zn-P framework is flexible and able to accommodate up to six Zn atoms per formula unit via bonding rearrangements, such as partial Zn/P substitution and the formation of Cu-Zn bonds. Such perturbations of the framework's bonding affect the thermal and charge transport properties. The overall thermoelectric figure-of-merit, ZT, of $Ba_8Cu_{14}Zn_2P_{30}$ is 0.62 at 800 K which is 9 times higher than the thermoelectric performance of the ternary parent phase $Ba_8Cu_{16}P_{30}$. Through a combination of inelastic neutron scattering and single crystal X-ray diffraction experiments at 10 K, low-energy rattling of the Ba guest atoms inside the large tetrakaidecahedral cages are shown to be the reason for the low thermal conductivities observed for the studied clathrates.

Introduction

Thermoelectric materials, which can convert waste heat into usable electrical energy, were originally developed for space applications. Currently, thermoelectrics are on demand for various terrestrial applications.[1-4] Such materials represent an intriguing challenge for materials chemists since a combination of incompatible properties is required to achieve high thermoelectric efficiency. Thermoelectric materials are expected to exhibit high thermopower, S, and electrical conductivity (low electrical resistivity, ρ) together with low thermal conductivity, κ.[5] The maximum value of a dimension-less thermoelectric efficiency, $ZT = S^2T/\rho\kappa$, where T is the absolute temperature, is widely used to compare materials' performances.[1-4] However, other characteristics, such as abundance, cost, the toxicity of starting materials, as well as the materials' overall performance and thermal stability in the desired temperature gradient, are crucial for real-life applications.[5] From a fundamental point of view, designing a material with a specific crystal structure, dopant distribution and concentration, and morphology allows one to overcome the strong coupling of the S, ρ, and κ.[1-5]

Proposed by Slack in 1995, the phonon-glass electron-crystal (PGEC) concept pointed out that clathrates, composed of 3D frameworks encapsulating large guest ions inside the oversized polyhedral cages, are promising thermoelectric materials, because the rattling of guest ions provides an intrinsically-low thermal conductivity for crystalline compounds.[6] Conventional clathrates with frameworks based on the tetrel elements, Si, Ge, and Sn are intensively investigated.[7,8] Our search for new thermoelectric materials is focused on the unconventional clathrates with a framework composed of late transition metals and phosphorus.[9-11] In a recent work, we scrutinized the structural aspects of a complex Zn substitution into the Cu sublattice of the $Ba_8Cu_{16}P_{30}$ clathrate-I.[12] A detailed investigation using synchrotron and neutron diffraction and pair distribution function analyses together with advanced electron microscopy studies revealed that the introduction of Zn into $Ba_8Cu_{16}P_{30}$ resulted in a collapse of the long-range ordered orthorhombic superstructure (Sp. Gr. *Pbcn*) to a locally-disordered cubic substructure (Sp. Gr. $Pm\overline{3}n$). This process was accompanied by the formation of Cu-Zn bonds in the framework. At high Zn

concentrations, >20% Zn/M_{total} (M = Cu + Zn), due to the separation of M and P atoms over different framework sites, partial ordering was observed.

In the present work, we report a comprehensive characterization of the electronic structure and chemical bonding in quaternary Ba-Zn-Cu-P clathrates-I, as well as transport properties and a description of the rattling of Ba guest atoms.

Experimental Details

Synthesis

All manipulations of the starting materials were performed inside an argon-filled glove box ($p(O_2)$ < 1 ppm). The starting materials, elemental metallic barium (Sigma-Aldrich, 99.9%), copper powder (Alfa Aesar, 99.99%), zinc shavings (Alfa Aesar, 99.8%), and red phosphorus (Alfa Aesar, 99%) were used as received. Details of the syntheses of the samples can be found elsewhere.[12] Single phase samples of $Ba_8Cu_{16-x}Zn_xP_{30}$ ($0 < x < 2.5$), $Ba_8Cu_{13.1}Zn_{3.3}P_{29.6}$, $Ba_8Cu_{12.5}Zn_4P_{29.5}$, and $Ba_8Cu_{11.4}Zn_{5.6}P_{29}$ were obtained from solid state reactions of the stoichiometric mixtures of elemental Ba, Cu, Zn, and P. Samples were placed into carbonized silica ampoules which were evacuated and flame-sealed. The ampoules were heated to 1173 K over 17 h, annealed at this temperature for 72 h, and cooled to room temperature. Products were reground in the glovebox and re-annealed 1173 K for 140 h, cooled down, reground in the glovebox and re-annealed under the same conditions for another 140 h. Finally, samples were melted to achieve full homogeneity at either 1223 K (x < 2.5) or 1173 K (x > 2.5).

Sample Densification and Transport Property Measurements

Powdered single phase samples were compacted using Spark Plasma Sintering (SPS 1050: Sumitomo Coal Mining Co, Ltd.). The polycrystalline samples were carefully ground into fine powders in the glovebox and then loaded in graphite dies. For the low temperature (5-400 K) measurements, 5 mm diameter graphite pressure dies with WC plungers were used. Samples were compacted at an applied temperature of 923 K (with overheat up to 943 K) and an overall pressure of 204 MPa. For the high-temperature measurements, 12.7 mm diameter graphite dies with graphite plungers were used at a higher sintering temperature, 950 K, with an applied uniaxial pressure of 80 MPa. The graphite and possible surface contamination were removed through polishing the surfaces of the pellets in a glovebox. The geometrical densities of pellets were above

90% of the theoretical X-ray densities, and they were well polished to a mirror-like shine. The samples purities after SPS were checked by powder X-ray diffraction, and no changes in the powder XRD patterns were observed from before and after SPS treatment. Low-temperature transport properties were characterized in the temperature range of 5-400 K using the commercial multipurpose Physical Properties Measurement System (PPMS, Quantum Design). The thermopower and thermal conductivity were measured using the Thermal Transport Option. The electrical resistivity was measured by a standard four-point alternating-current technique to exclude the resistance of the leads. High-temperature transport properties in the temperature range 300-873 K were performed using Netzsch LFA457 and Linseis LSR-3/1100 instruments. In the thermal conductivity measurements, a standard sample of pyroceram 9606 was used as the reference for measuring the heat capacity. The thermal conductivity was calculated from: $\kappa = D \times \rho \times C_P$ (D: thermal diffusivity; ρ: density; C_P: heat capacity). After the thermal conductivity measurements were completed, the same pellets were cut into bars of suitable sizes to perform the thermopower and electrical conductivity measurements.

Solid State NMR

All ^{31}P Magic-Angle-Spinning nuclear magnetic resonance (MAS NMR) spectroscopic measurements were carried out using a 2.5 mm Bruker CP/MAS probe and a Bruker Avance 500 spectrometer, operating at a magnetic field of 11.7 T, corresponding to a ^{31}P Larmor frequency of 202.4 MHz. The polycrystalline samples were mixed in a 1:1 ratio with SiO_2 before loading into a 2.5mm ZrO_2 rotor to ensure stable spinning. Each spectrum was obtained by Fourier transformation of an average of 720-1024 free induction decays (FID) collected using a 60° pulse (1.23 μs) and a recycle delay of 1.5s. The ^{31}P chemical shifts were externally referenced to that of a solution of 85% H_3PO_4 (δ_{iso} = 0 ppm).

Density of States Calculations

Density of states calculations were performed with CASTEP using Materials Studio to generate input files from the initial cif files. Perdew-Burke-Ernzerhof generalized gradient approximation calculations (GGA-PBE) were performed for the select compositions using ultrasoft potentials with a 2×2×1 *k*-point grid, after a fine geometry optimization of the structures.[13] For geometry optimizations, the following values were used: plane-wave energy cutoff = 440 eV, electronic energy tolerance = 5×10^{-10} eV/atom, geometric energy tolerance = 5×10^{-9} eV/cell, geometric force

tolerance = 0.005 eV/Å, geometric stress tolerance = 0.001 (GPa), geometric displacement tolerance = 5×10^{-4} Å, and maximum iterations = 500.

Phonon Density of States and Inelastic Neutron Scattering Calculations

Phonon density of states calculations were performed with CASTEP using Materials Studio.[14] A calculation for $Ba_8Cu_{16}P_{30}$ was performed using an orthorhombic unit cell. A calculation for $Ba_8Cu_{13}Zn_3P_{30}$ was performed using a cubic model converted to lower symmetry, by assigning three out of 16 metal atoms to be Zn for randomly-chosen sites. For phonon density of states calculations, finite displacements were used. For the orthorhombic and cubic systems, phonon sampling *k*-meshes of 2×2×1 and 3×3×3 were used, respectively. aCLIMAX was used to convert the calculated phonon density of states to calculated inelastic neutron scattering spectra.[15]

Inelastic Neutron Scattering (INS) Measurements

Samples of $Ba_8Cu_{16}P_{30}$ and $Ba_8Cu_{13.1}Zn_{3.3}P_{29.6}$ were synthesized in 5g quantities for the INS measurements. Data were collected using the indirect-geometry spectrometer VISION at the Spallation Neutron Source, Oak Ridge National Laboratory. Powders were packed into aluminum cans. Data were collected in the temperature range 5-150 K. The empty sample can was also measured, and the background spectrum was subtracted from the total spectra.

Low-Temperature Single Crystal X-ray diffraction

Single crystal X-ray diffraction experiments were carried out at 10 K using a Bruker AXS SMART diffractometer with an APEX-II CCD detector and MoK_α radiation. A stream of He gas was used to achieve a 10 K temperature. The datasets were recorded as ω-scans at 0.4° step width and integrated with the Bruker SAINT software package.[16] Multiscan absorption corrections were applied due to the irregular shapes of the crystals. The solutions and refinements of the crystal structures were carried out using the SHELX suite of programs.[17] Since Cu and Zn atoms are indistinguishable via single crystal X-ray diffraction, refinements of all compositions were performed with only Cu or P in the framework sites. The framework positions were refined as mixed occupancy Cu/P positions with two constrains: i) equivalent atomic displacement parameters for Cu and P, and ii) 100% total occupancy of each framework site. Difference electron density plots were calculated using JANA2006 software.[18] To achieve the chemically-reasonable composition, the Zn content was calculated from the refined P content assuming an electron-

balanced composition. 2.4 Zn atoms per formula unit were distributed to 6*c* and 16*i* framework sites and not further refined. In the split position model, the refined coordinates of Ba2 are [0.2492(14), 0.5128(4), 0]. Further details of the crystal structure determination may be obtained from either Fachinformationszentrum Karlsruhe, Germany, by quoting the depository number CSD-434087 or in the Cambridge Crystal or Cambridge Crystallographic Data Centre by quoting the depository number CCDC-1819462.

Results and Discussion

Our detailed structural characterization showed that the chemical bonding, *i.e.* the formation of Cu-Zn bonds, in the framework of the Ba-Cu-Zn-P clathrates-I results in a substantial alteration of the crystal structure.[12] The parent Zn-free structure of $Ba_8Cu_{16}P_{30}$ crystallizes in the orthorhombic superstructure of clathrate-I, $2\sqrt{2} \times 1 \times \sqrt{2}$, space group *Pbcn,* with 8 Cu and 15 P crystallographically-independent sites. Quaternary clathrates $Ba_8Cu_{16-x}Zn_xP_{30}$ with $x < 2$ crystallize in the same structure and Zn atoms are located in Cu positions. A further increase in the Zn content results in the collapse of the orthorhombic structure of $Ba_8Cu_{14}Zn_2P_{30}$ into a cubic clathrate-I cell, $1 \times 1 \times 1$ space group $Pm\overline{3}n$ with only three crystallographically-independent sites, each of which is jointly occupied by Cu, Zn, and P. We investigated the relationships between the bonding, electronic, and transport properties of the Ba-Cu-Zn-P clathrates-I.

Electronic Structure

To better understand the impetus for the structural conversions occurring in the Zn-substituted $Ba_8Cu_{16}P_{30}$ system, electronic structure calculations were performed using compositional models based on different Ba-Cu-Zn-P stoichiometries and unit cells symmetries. We have shown that orthorhombic $Ba_8Cu_{16}P_{30}$ is a *p*-type metal with the Fermi level located in the conduction band.[19] According to Zintl electron count, the addition of 2 electrons should make this compound electron balanced. This was proven by electronic structure calculations of the orthorhombic $Ba_8Cu_{14}Zn_2P_{30}$ composition.[12] Zintl electron count predicts that for the same structure, increasing the Zn content over 2 should result in *n*-type metallic materials with the Fermi level located in the conduction band. To verify this prediction, we calculated the electronic structure of two Zn-rich orthorhombic compositions $Ba_8Cu_{12}Zn_4P_{30}$ and $Ba_8Cu_{10}Zn_6P_{30}$. Contrary to Zintl electron count predictions, both compositions are calculated to be semiconductors (Figure 1). The clathrate framework relaxes to accommodate the extra electrons by the breaking of several P-P bonds (Figure 2). This agrees with the electron count considerations, since each 3-coordinated P atom requires an extra electron to realize an electron octet configuration. A similar framework relaxation mechanism was found experimentally in Ge- and Sn-based clathrates.[20-23] This illustrates that the Cu-Zn-P clathrate framework is flexible and may relax to accommodate excess electrons by an alteration of its chemical bonding in the framework.

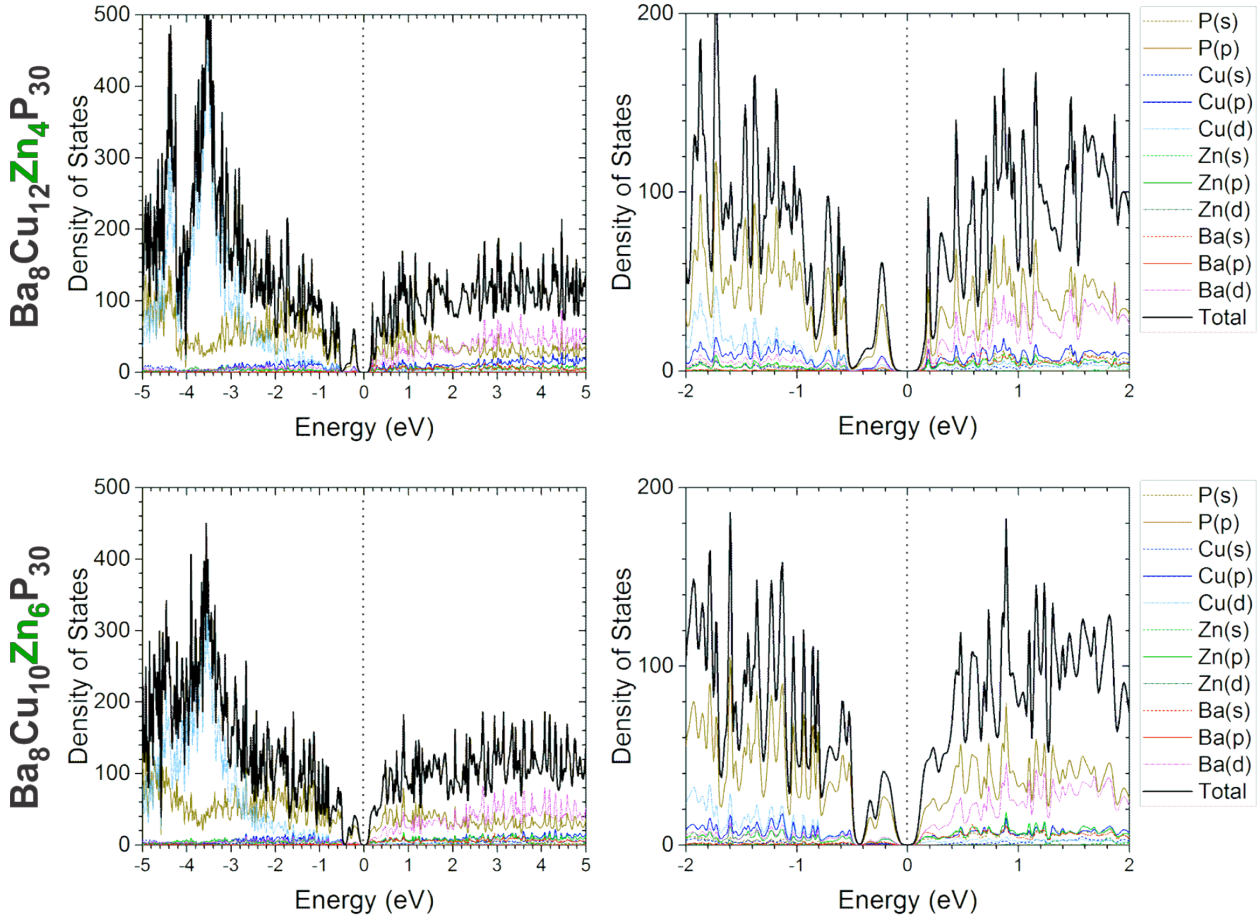

Figure 1. Calculated densities of states for orthorhombic compositions (top) $Ba_8Cu_{12}Zn_4P_{30}$ and (bottom) $Ba_8Cu_{12}Zn_6P_{30}$. Zoomed-in views of the calculated densities of states are shown in the right-hand panels. The fermi level is shown with vertical dotted line.

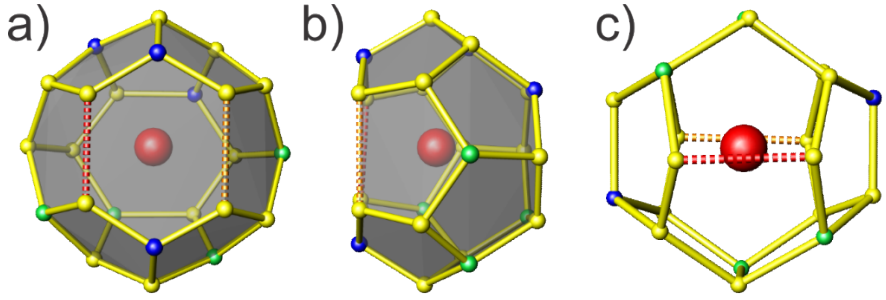

Figure 2. The results of a geometry optimization on the orthorhombic ordered $Ba_8Cu_{10}Zn_6P_{30}$ model. The calculated distortion leads to the elongation of two P bonds, indicated by dashed lines (red = 3.26 Å, orange = 3.07 Å) for the tetrakaidecahedra (a and b) as well as the pentagonal dodecahedra (c). Cu: green; Zn: blue; P: yellow.

Despite the calculated results of geometry optimizations, the experimental diffraction studies[12] reveal no elongated, > 3 Å, chemical bonds in the Ba-Cu-Zn-P clathrates with more than two Zn atoms. Instead, a different relaxation mechanism takes place. To accommodate the extra electrons,

the *M*/P (M = Cu,Zn) ratio is increased by additional Zn/P substitution. This process is accompanied by the formation of Cu-Zn bonds in the framework. In the aforementioned theoretical orthorhombic compositions $Ba_8Cu_{12}Zn_4P_{30}$ and $Ba_8Cu_{10}Zn_6P_{30}$, every metal atom is surrounded by four P atoms and there are no Cu-Zn bonds. To model Cu-Zn bonding we calculated several compositions with 0, 1, and 2 M-M bonds (M = Cu, Zn). Those calculations demonstrate that the formation of M-M bonds has a significant impact on the clathrates electronic structures. Unfortunately, the geometry optimizations resulted in the stretching of certain framework bonds to 2.86 Å for M-M and 2.91 Å for P-P, and such results cannot be used for a quantitative comparison with the experimental data. On the qualitative level, a comparison of the models with and without M-M bonds with the same composition demonstrates that M-M bonding significantly alters the DOS in the vicinity of the Fermi level. As such, a strong dependence of the electronic properties on the Zn content is expected in the Ba-Cu-Zn-P clathrates-I.

^{31}P Solid state NMR

Chemical bonding in the Ba-Cu-Zn-P clathrates-I was analyzed by means of ^{31}P solid state NMR spectroscopy (Figures 3,4) which is a useful tool for analysis of framework thermoelectrics.[11,24-27] In the crystal structure of $Ba_8M_{16}P_{30}$, which is an orthorhombic superstructure of clathrate-I, there are 15 crystallographically-independent P sites.[28] The ^{31}P MAS NMR spectra of the $Ba_8Cu_{16}P_{30}$ sample (Figure 3) resemble those of an isostructural Au-containing analogue,[27] with a strong paramagnetic shift due to the interaction of the conduction electrons with P nuclear spins. However, the nature of the transition metal plays a significant role in chemical bonding of metal-phosphorus clathrates. For $Ba_8Au_{16}P_{30}$ the experiments performed at varied spinning frequencies resolved four main ^{31}P contributions at 755, 518, 342, and 332 ppm.[27] The ^{31}P MAS NMR spectra of $Ba_8Cu_{16}P_{30}$ display higher resolution, and experiments performed at different spinning frequencies resolve at least 8 resonances with chemical shifts of 600, 577, 543, 360, 206, 160, 141, and 131 ppm. In general, chemical shifts at lower ppm values indicate a lower charge carrier concentration. In the electron-balanced phosphides, the ^{31}P chemical shifts are smaller than 100 ppm.[11,24,29,30] One of the reasons for the difference in the charge carrier concentrations between $Ba_8Cu_{16}P_{30}$ and $Ba_8Au_{16}P_{30}$ is the nature of P atoms participating in the longest P-P distance in the framework, 2.46 Å in the Cu-containing compound and 2.72 Å in the Au-containing one. The former distance is longer than the usual covalent P-P bond (2.3-2.3 Å),[31-35] but such long distances are not uncommon in different transition metal phosphides, such as NiP (2.43 Å), ZrP_2 (2.41 Å),

CeP_2 (2.40-2.45 Å), and $LaCuP_2$ (2.2-2.47 Å).[36-39] P-P distance of 2.72 Å in the Au-containing analogue is too long for the covalent interaction and P atoms participating in such bonding should be considered as three-coordinated.

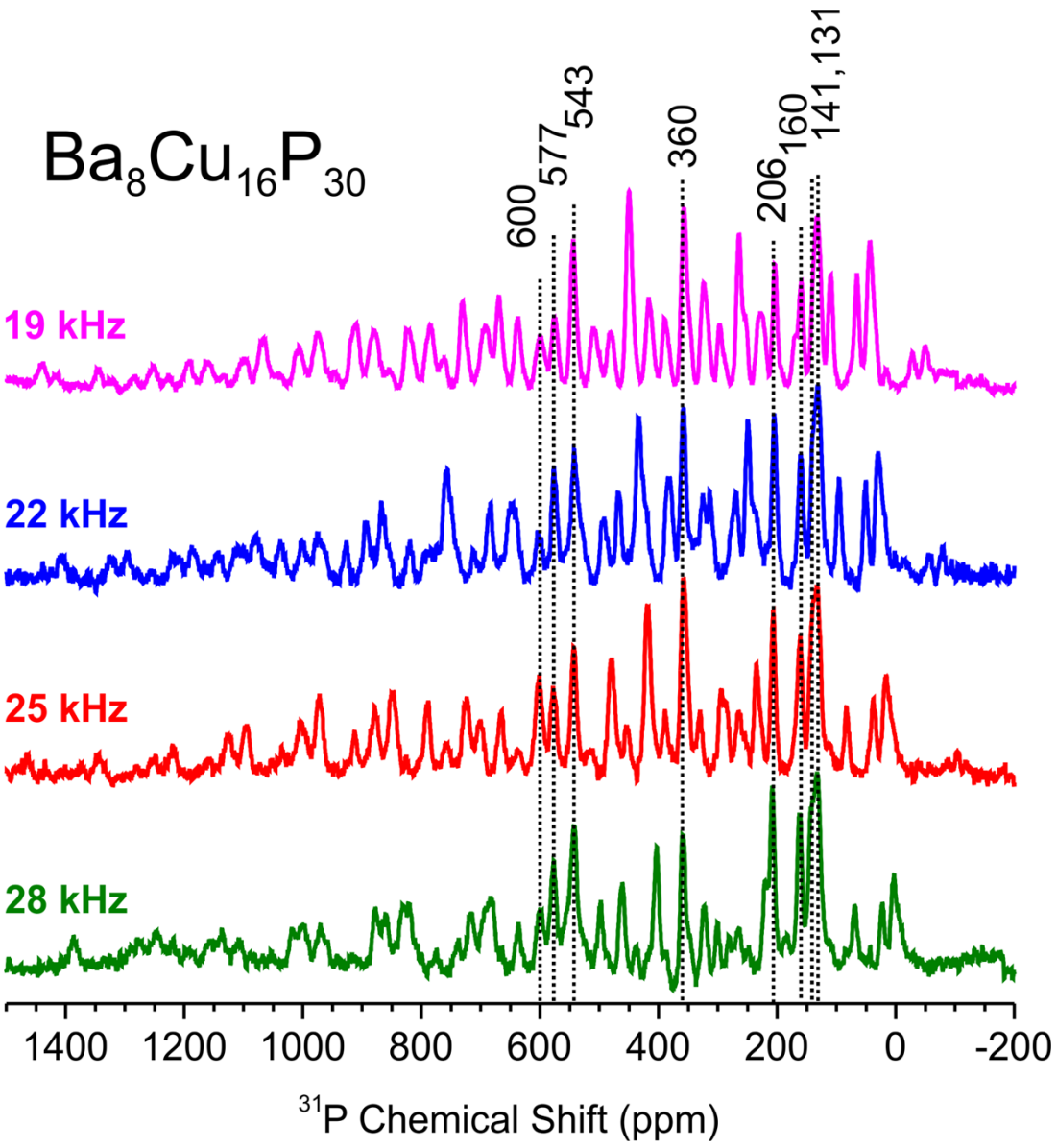

Figure 3. ^{31}P MAS NMR experimental spectra of $Ba_8Cu_{16}P_{30}$ collected at the indicated spinning frequency in the range of 19-28 kHz. Isotropic chemical shifts are shown with dotted lines, the other peaks are multiple sidebands.

^{31}P MAS NMR spectra of the quaternary Ba-Cu-Zn-P clathrates-I revealed several clear trends (Figure 4). The incorporation of Zn introduces a disorder in the framework, resulting in broad unresolved peaks. Moreover, Zn incorporation reduces the total carrier concentration as compared

to $Ba_8Cu_{16}P_{30}$, resulting in a significant reduction in the ^{31}P chemical shift. For $Ba_8Zn_1Cu_{15}P_{30}$, the main ^{31}P signal is observed at 82 ppm, while for samples with two and three Zn atoms in the framework, the chemical shift is centered around 16 ppm. This is in accordance with the measured transport properties, indicating an overall reduction of the charge carrier concentration upon introduction of Zn atoms (*vide infra*).

NMR studies of the sample with the highest Zn content, $Ba_8Cu_{11.4}Zn_{5.6}P_{29}$, further confirmed the presence of a superstructure with partial ordering caused by the separation of *M* and P positions in the clathrate framework, as proposed from the earlier diffraction and microscopy experiments.[12] While Cu/Zn disorder is still present, resulting in broad NMR lines, the appearance of an additional component at a significantly lower chemical shift of –160 ppm is obvious (Figure 4). Spectra collected at multiple spinning frequencies for this sample are shown in Figure 4 right. A similar distribution of P signals ranging from +5 to –202 ppm was observed for the $Ba_8M_{24}P_{28+\delta}$ (M = Zn,Cu) clathrate compound with the separation of M and P atoms over different 4-, 5-, and 6-coordinated framework positions.[11]

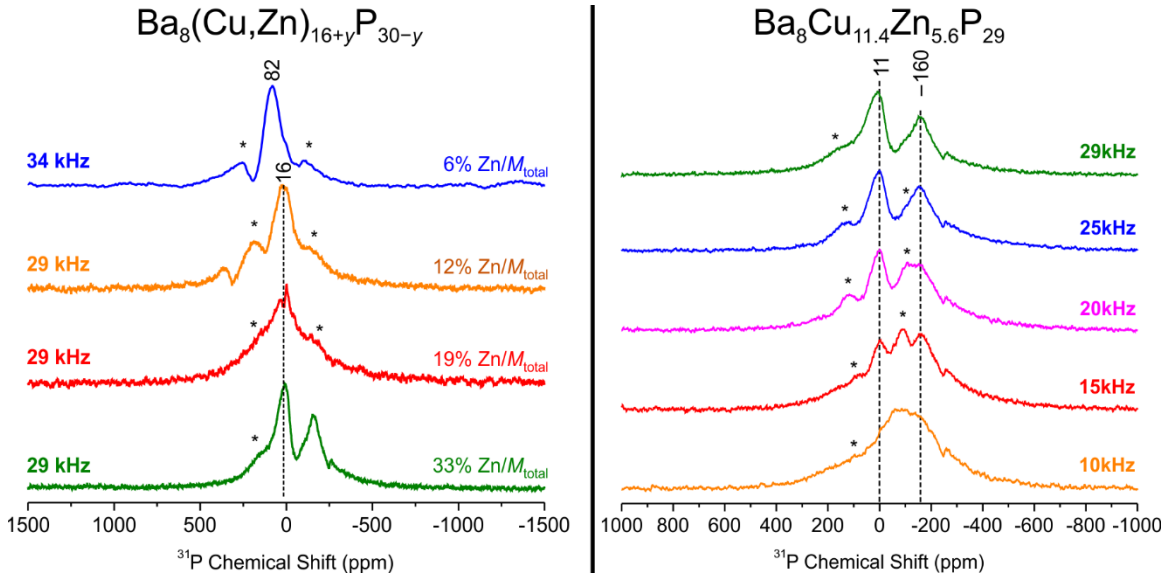

Figure 4. Left: ^{31}P MAS NMR experimental spectra of Ba-Zn-Cu-P clathrates-I with different Zn contents indicated in % of Zn/M_{total}, M_{total} = Cu+Zn; color code matches Figures 5 and 6. Right: ^{31}P MAS NMR experimental spectra of $Ba_8Cu_{11.4}Zn_{5.6}P_{29}$ collected at the indicated spinning frequency in the range of 10-29 kHz. Isotropic chemical shifts are shown with dashed lines; sidebands are shown with asterisks.

Transport Properties

The low temperature transport properties of select Ba-Cu-Zn-P clathrate-I samples with 0%, 3%, 9%, 12%, 13%, 19%, 25%, and 33% of Zn/M_{total} are shown in Figures 5 and 6.

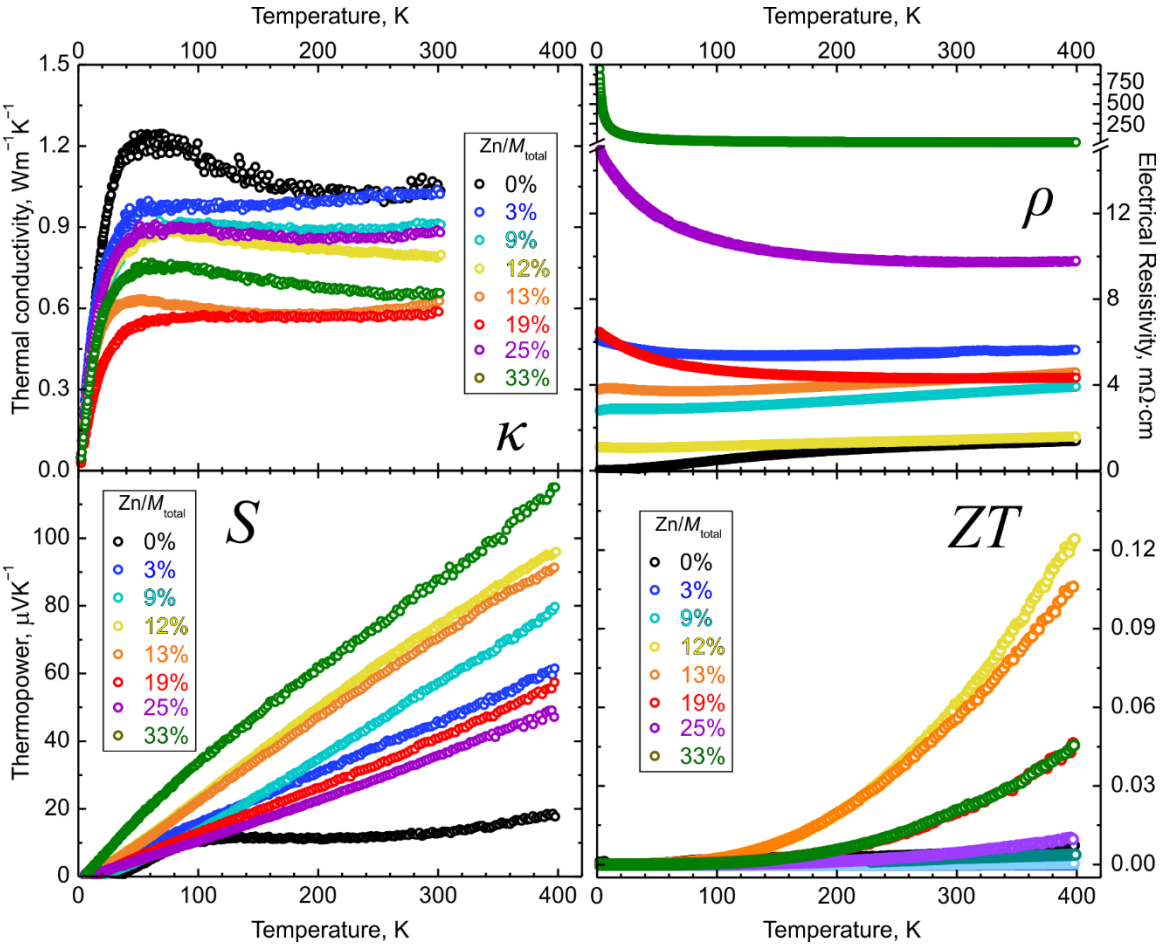

Figure 5. Low-temperature thermoelectric properties for selected samples of $Ba_8M_{16+y}P_{30-y}$, M = Cu, Zn. The Zn content is shown in % from M_{total} = Cu+Zn. Thermal conductivity: top left; thermopower: bottom left; electrical resistivity: top right; ZT: bottom right. Note the break in the resistivity plot due to the high values measured for the 33% Zn/M_{total} composition.

There are several overlapping trends in the transport properties. Compositions with 0 < Zn/M_{total} < 12% crystallize in an ordered orthorhombic superstructure, and an increase in the Zn content causes a decrease in the charge carrier concentration, as emphasized by the increase in thermopower. A crossover from the orthorhombic superstructure to the cubic substructure occurs for compositions with Zn/M_{total} = 12-13% which are the closest to electron-balanced. Samples with Zn/M_{total} = 12-13% exhibit high thermopowers due to their lower charge carrier concentrations,

and their nearly temperature-independent resistivities, $\rho_{300\,K}/\rho_{2\,K} = 1.3$ for both samples: typical behavior for heavily-doped semiconductors and semimetals. A further increase in the Zn content resulted in the formation of Zn-Cu bonds in the framework and an adjustment of the *M*/P content, leading to a decrease in the thermopower and an increase in the resistivity. According to our NMR and diffraction experiments, the $Ba_8Cu_{11.4}Zn_{5.6}P_{29}$ sample (33% Zn/M_{total}) has a trigonal ordered superstructure.[12] This phase exhibits semiconducting properties, including the highest thermopower and a typical thermal activation behavior of its electrical resistivity with values significantly higher than those for all other studied samples (Figure 5).

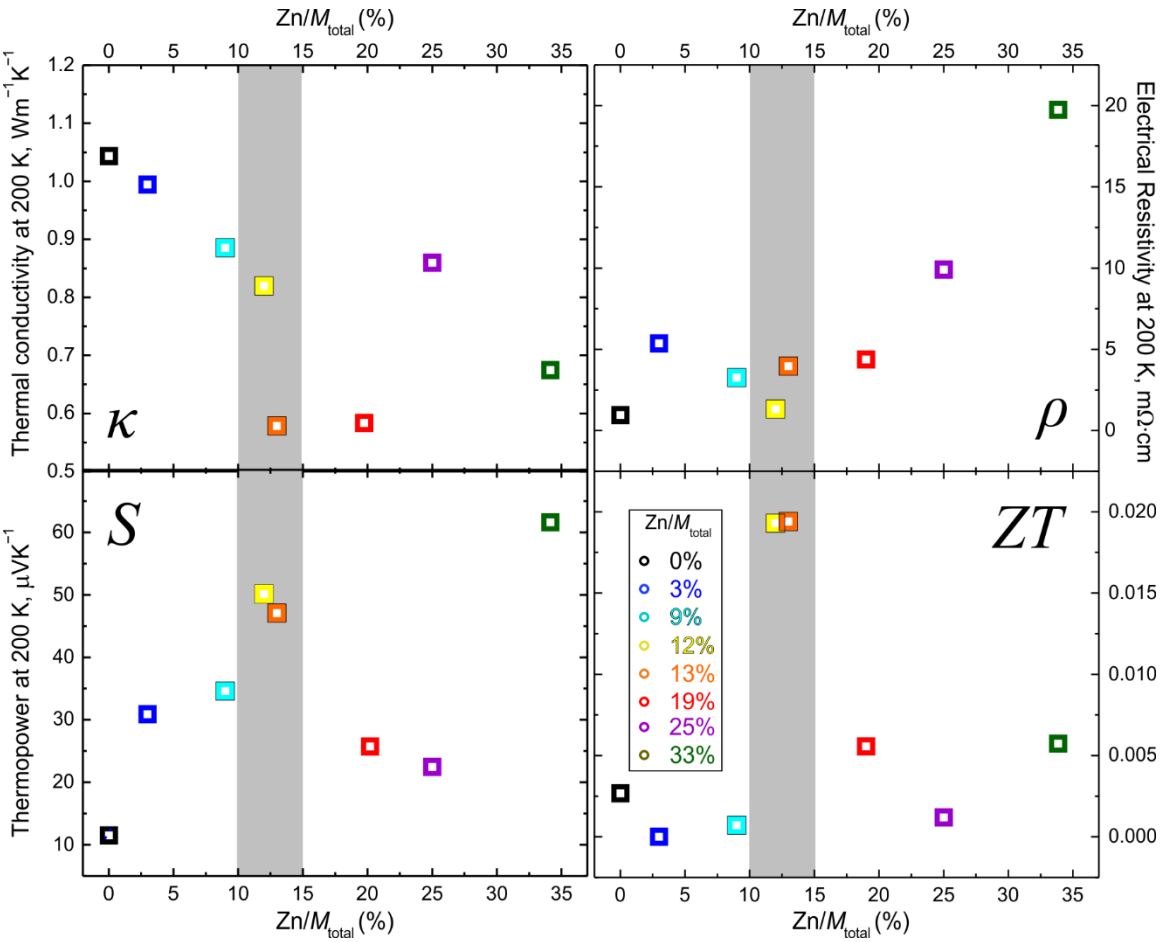

Figure 6. Thermoelectric properties for selected samples of $Ba_8M_{16+y}P_{30-y}$, M = Cu, Zn, at 200 K. Thermal conductivity: top left; thermopower: bottom left; electrical resistivity: top right; ZT: bottom right. The approximate multiphase region (orthorhombic + cubic) around $Ba_8Cu_{14}Zn_2P_{30}$ is shaded. Color of the symbol is consistent with Figure 5.

The thermal conductivities of clathrates are usually low, often below 3 $Wm^{-1}K^{-1}$.[7-9] In the studied samples, the thermal conductivities are lower than those of many other known

clathrates. Each of the Zn-substituted systems has a thermal conductivity below 1.3 $Wm^{-1}K^{-1}$. The lower thermal conductivity of the Zn-substituted phases compared to $Ba_8Cu_{16}P_{30}$ are due to two reasons: i) a decrease in the electronic contribution to the total thermal conductivity (Figure S1); and ii) local disorder in the cubic framework for samples with >12% Zn/M_{total}. A combination of the highest thermopower and ultra-low thermal conductivity with moderate electrical resistivity resulted in the *ZT* of 0.12 at 400 K for $Ba_8Cu_{14}Zn_2P_{30}$. This composition was selected for the high-temperature thermoelectric characterization (Figure 7).

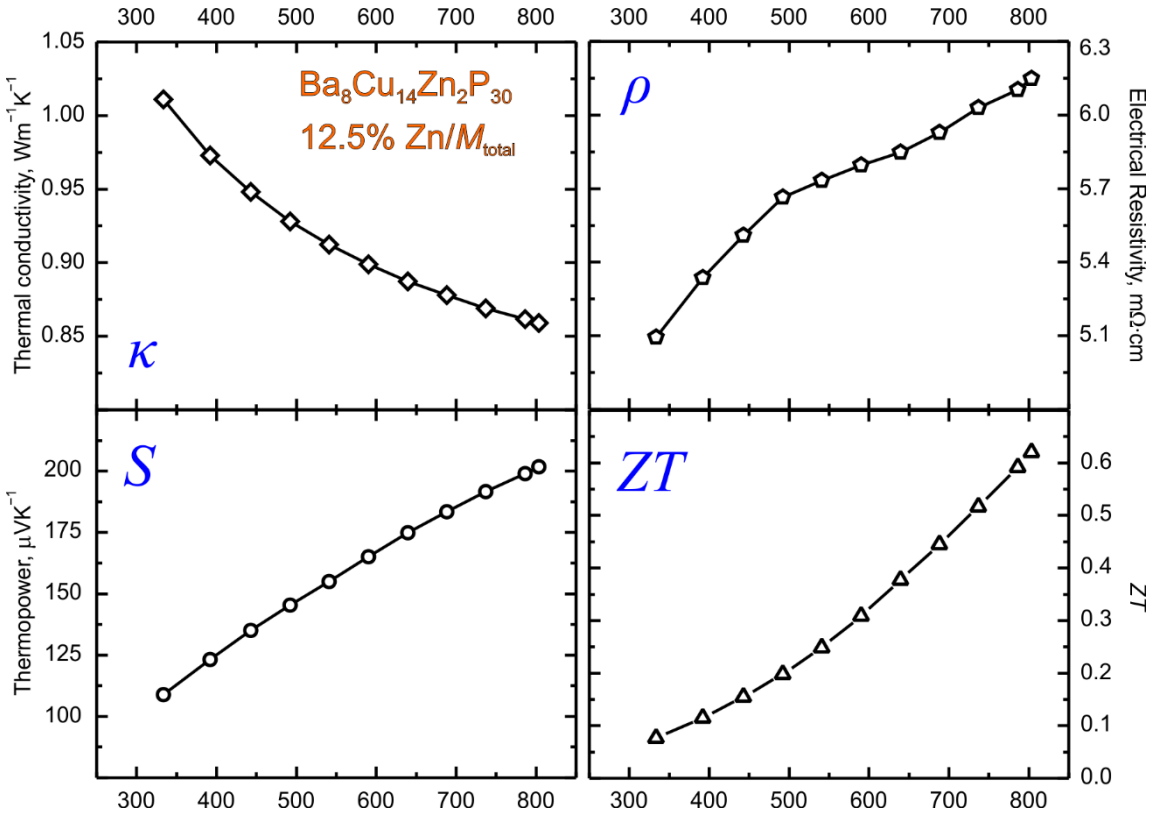

Figure 7. High-temperature thermoelectric properties for $Ba_8Cu_{14}Zn_2P_{30}$, 12.5% Zn/M_{total}. Thermal conductivity: top left; thermopower: bottom left; electrical resistivity: top right; ZT: bottom right.

High-temperature properties measurements confirmed the trends observed at low-temperatures. Thermopower almost linearly increases, reaching 200 μVK^{-1} at 800 K. Electrical conductivity exhibits an almost temperature-independent behavior typical for semi-metals or heavily-doped semiconductors, with a slight increase over 500 K: $\rho_{800\,K}/\rho_{300\,K}$ = 1.2. The room-temperature thermal conductivity is higher than that observed in the low-temperature measurements on the PPMS. This type of discrepancy between two different applied methods is typical.[19,40] The overall

thermoelectric figure-of-merit, *ZT*, of $Ba_8Cu_{14}Zn_2P_{30}$ is 0.62 at 800 K. This is 9 times higher than the performance of the Zn-free $Ba_8Cu_{16}P_{30}$, and it is comparable to the thermoelectric performance of another clathrate with Cu-P framework, $Ba_8Cu_{14}Ge_6P_{26}$.[19]

Inelastic Neutron Scattering and Phonon Density of States

To understand the low thermal conductivities of the new Zn-substituted, unconventional clathrates and their structural relationships, vibrational properties were characterized. Inelastic neutron scattering (INS) experiments were conducted for $Ba_8Cu_{16}P_{30}$ and $Ba_8Cu_{13.1}Zn_{3.3}P_{29.6}$ samples at the VISION Beamline at Oak Ridge National Lab. INS can probe the phonon density of states of solids, painting a picture of the number, density, and spread of phonon modes in the system.[41-44] Experimental and calculated INS spectra for $Ba_8Cu_{16}P_{30}$ and $Ba_8Cu_{13.1}Zn_{3.3}P_{29.6}$ are shown in Figure 8. Variable-temperature INS showed no significant differences in the spectra collected at different temperatures, except for minor changes in peak intensities that can be associated with the phonon population effect and Debye-Waller factor (Figure S2). For the calculation of $Ba_8Cu_{16}P_{30}$, an ordered orthorhombic cell was used. In the calculation of $Ba_8Cu_{13.1}Zn_{3.3}P_{29.6}$, a cubic model with an idealized $Ba_8Cu_{13}Zn_3P_{30}$ composition was used by converting the cell to lower symmetry and assigning an appropriate number of each atom to randomly-chosen sites. Because two models of different symmetry were used, some changes in the calculated spectra are due to the replacement of Zn with Cu, and some may be due to the differences in symmetry. To evaluate the relative contributions of those factors a huge number of low-symmetry model should be computationally investigated which is outside the scope of current investigation.

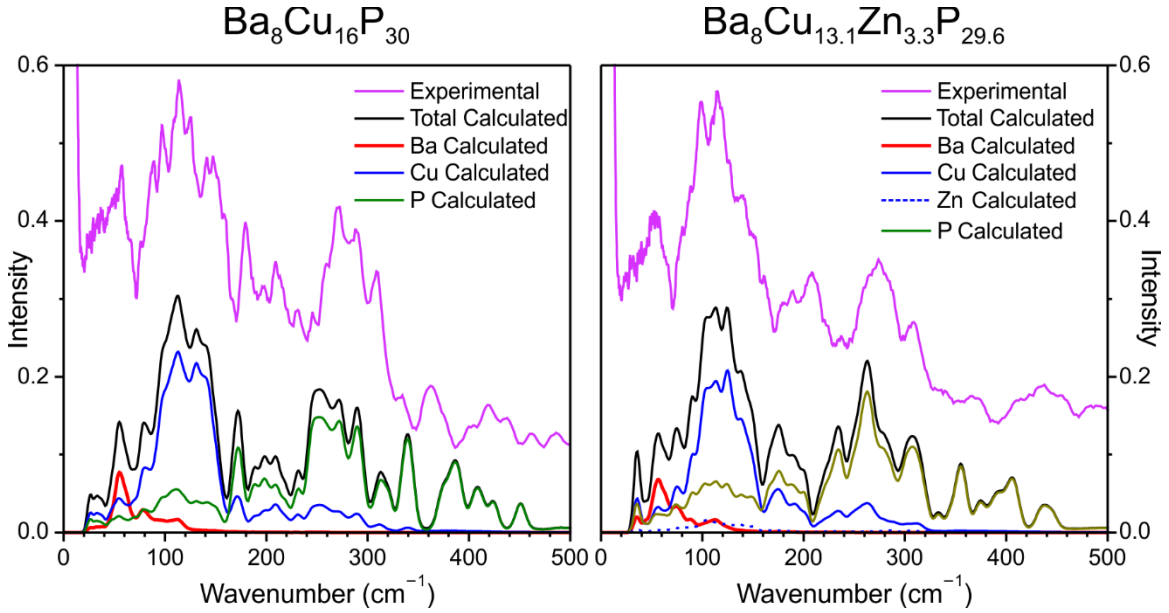

Figure 8. Experimental and calculated inelastic neutron scattering (INS) spectra for $Ba_8Cu_{16}P_{30}$ (left) and $Ba_8Cu_{13}Zn_3P_{30}$ (right).

The calculated spectra of both phases match the experimental spectra remarkably well. Both spectra have low energy Ba contributions at around 55 cm^{-1} related to the vibrational movement of Ba atoms inside tetrakaidechadra in a plane parallel to the large six-membered faces (Figure S3). These sharp contributions are similar to contributions reported for tetrel clathrates which correspond to the rattling or off-center displacement of guest atoms in the large cages. Similar contributions in tetrel clathrates have been shown to induce an avoided crossing of the host frameworks' acoustic phonons (with high group velocity, and thus large contributions to the thermal conductivity) and the guest's optical phonon bands, contributing to the overall low thermal conductivities of the clathrates.[45] Calculations of both models show a small, but non-zero, low energy contribution of the framework atoms to the states below 40 cm^{-1}. This indicates that framework substitutions in the tetrel-free clathrates may impact the thermal conductivity. However, our calculations were only performed for one possible model of each compound and they may not completely represent the actual phonon dispersion.

The Vibrational Behavior of Ba Guests

To further characterize the rattling dynamics of the Ba guest atoms, we turned to experimental diffraction measurements. The vibrational behavior of Ba guest atoms located inside large tetrakaidecahedral cages was studied by a low temperature single crystal X-ray diffraction

experiment. The experiment was performed at 10 K on a cubic crystal with the refined composition $Ba_8M_{16.1}P_{29.9}$, M = Cu,Zn. The electron density distribution for Ba atoms inside the tetrakaidodecahedral cages, position 6*d* (¼; 0; ½) was not spherical, but has four pronounced maxima (Figure 9a). The electron density for this Ba position can alternatively be described as either the anisotropic Ba atom in the center of the cage (Figures 9b and 9d), or a partially occupied position 24*k* (0.2508(14); 0.0128(4); ½) forming a square around the center of the cage (Figures 9c and 9e), corresponding to the electron density maxima found in Figure 9a. In such a description, Ba-Ba distances are 0.182(7) Å and 0.256(8) Å and the square plane is parallel to the hexagonal faces of the tetracaidecahedron (Figure 9e). Note that in the case of anisotropic refinement, the atomic displacement parameter for Ba atoms inside the tetrakaidodecahedral cage, position 6*d* (¼; 0; ½), was significantly larger that of other atoms (Table S1). This investigation points to the off-centering of Ba atoms inside the large tetrakadecahedral cages which is consitent with INS studies and the glass-like behavior of the thermal conductivity. Similar off-centering of Ba or Eu gust cations inside large tetrakaidecahedra composed of Ga and Ge was also observed for tetrel-clathrates.[46-49]

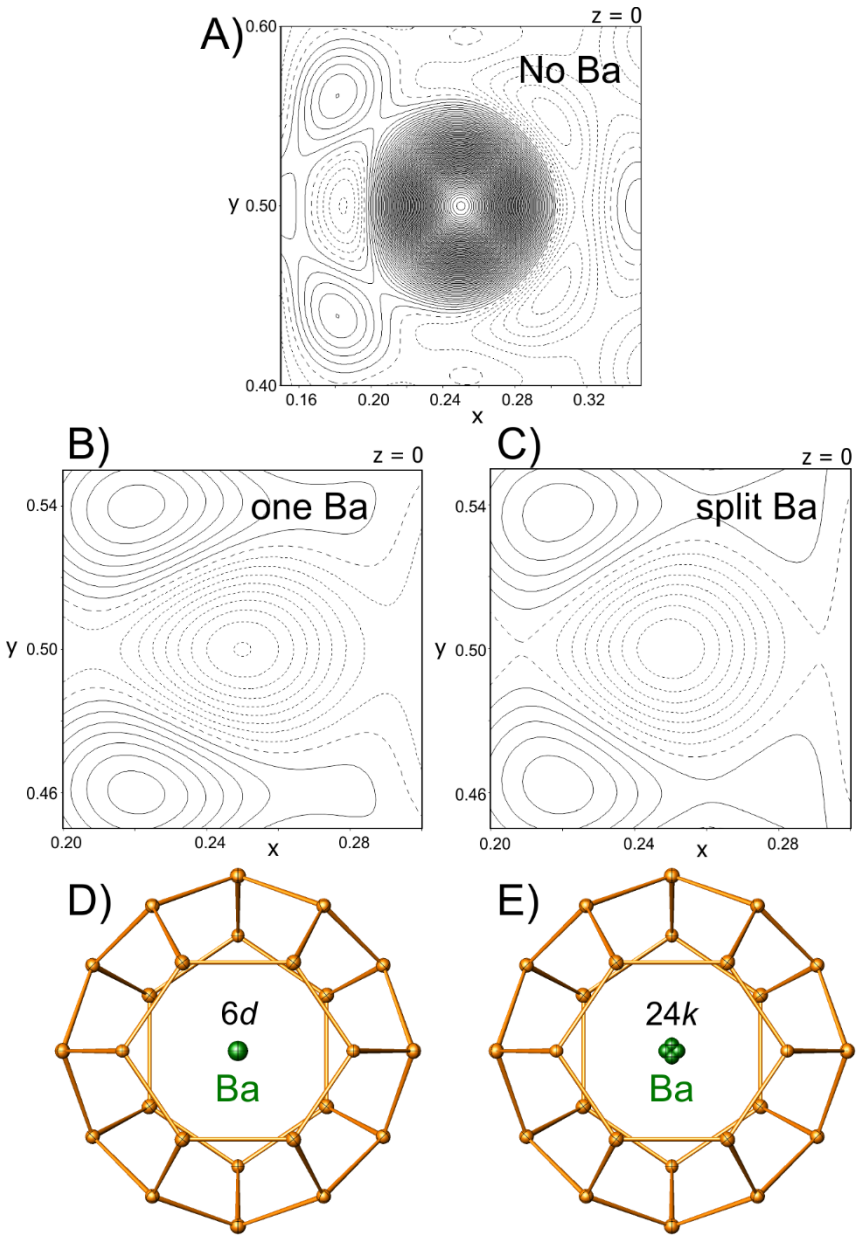

Figure 9. The refinements of the cubic (Sp. Gr. $Pm\bar{3}n$) crystal structure of $Ba_8M_{16.1}P_{29.9}$ clathrate (M = Cu,Zn) from the single crystal diffraction data collected at 10 K. A: total electron density in the vicinity of the Ba2 position, isolines are shown with step of 2 e/Å^3, solid isolines – positive density, dashed isolines – negative density; B and C: difference electron densities for anisotropic refinement of one Ba position in the center of the cage and isotropic off-centered refinements with 4 split positions, isolines are shown with step of 0.2 e/Å^3. D and E: corresponding structural images with ellipsoids drawn with 50% probability. All other atoms are refined anisotropically in both models. Ba: green; framework atoms: orange.

Conclusions

Our characterization of the electronic structure and chemical bonding of quaternary clathrate-I phases with the overall composition $Ba_8M_{16+y}P_{30-y}$ (M = Cu,Zn) demonstrated that the Cu-Zn-P framework is flexible and able to accommodate up to six Zn atoms without a substantial increase in valence electron concentration, mainly due to the bonding rearrangements, such as partial Zn/P substitution and the formation of Cu-Zn bonds. Such rearrangements have drastic impacts on the transport properties. A classical semiconducting behavior was achieved only for the sample with maximum Zn content where diffraction and ^{31}P solid-state NMR investigations detected M/P ordering in the framework. Due to its high electrical resistivity, this sample does not exhibit the highest thermoelectric performance Instead, the sample with 2 Zn atoms per formula unit does, demonstrating ZT = 0.62 at 800 K, almost an order of magnitude improvement compared to the performance for the Zn-free parent compound, $Ba_8Cu_{16}P_{30}$. Furthermore, inelastic neutron scattering measurements and low-temperature X-ray diffraction experiments explain the ultralow thermal conductivity of the studied phases by the low energy rattling of Ba guest atoms located inside large tetrakaidecahedral cages. By detailed investigations of the Zn substitution in the $Ba_8Cu_{16}P_{30}$ clathrate-I, we have shown that unconventional clathrates with transition metal-phosphorus frameworks exhibit promising thermoelectric properties combined with high thermal stabilities and property tunability.

Acknowledgements

The authors wish to thank Dr. S.M. Kauzlarich for use of SPS, LFA, and LSR-3 equipment; and Dr. Håkon Hope and Dr. James Fettinger for help with 10 K diffraction experiments.

AUTHOR INFORMATION

Corresponding Author: kovnir@iastate.edu

Author Contributions

All authors have given approval to the final version of the manuscript.

Authors declare no competing financial interests.

Funding Sources

This research was supported by the U.S. Department of Energy, Office of Basic Energy Sciences, Division of Materials Sciences and Engineering under Award DE-SC0008931. J.D. acknowledges the DOE-SCGSR fellowship for time spent at Oak Ridge National Laboratory. This research used resources at the Spallation Neutron Source operated by the Oak Ridge National Laboratory which is sponsored by the Scientific User Facilities Division, Office of Basic Energy Sciences, U.S. Department of Energy.

Supporting Information

Variable-temperature INS spectra, a graph with relative contributions of electronic and lattice terms to the total thermal conductivity, a table with anisotropic displacement parameters for the 10 K single crystal X-ray diffraction experiment, and a demonstration of the rattling modes of Ba atoms.

References

1. Tan, G.; Zhao, L.-D.; Kanatzidis, M. G. Rationally Designing High-Performance Bulk Thermoelectric Materials. *Chem. Rev.* **2016,** *116,* 12123-12149.

2. Zeier, W. G.; Zevalkink, A.; Gibbs, Z. M.; Hautier, G.; Kanatzidis, M. G.; Snyder, G. J. Thinking Like a Chemist: Intuition in Thermoelectric Materials. *Angew. Chem. Int. Ed.* **2016,** *55,* 2-18.

3. Bux, S. K.; Fleurial, J.-P.; Kaner, R. B. Nanostructured materials for thermoelectric applications. *Chem. Commun.* **2010,** *46,* 8311-8324.

4. Owens-Baird, B.; Heinrich, S.; Kovnir, K. Thermoelectric Materials. *Encyclopedia of Inorganic and Bioinorganic Chemistry.* **2017,** *DOI: 10.1002/9781119951438.eibc2497,* 1-35.

5. Thermoelectrics Handbook: Micro to Nano; Rowe, M., Ed. Taylor&Francis: Boca Raton, FL, **2006**.

6. Slack, G. A. New Materials and Performance Limits for Thermoelectric Cooling in: D.M. Rowe, Ed., CRC Handbook of Thermoelectrics, CRC, Boca Raton, 1995, pp. 407–440.

7. Dolyniuk, J.; Owens-Baird, B.; Wang, J.; Zaikina, J. V.; K. Kovnir, K. Clathrate thermoelectrics. *Mat. Sci. Eng. R.* 2016, **108**, 1-46.

8. The Physics and Chemistry of Inorganic Clathrates, Ed. Nolas, G. S. Springer: Philadelphia, New York, **2014**.

9. Wang, J.; Dolyniuk, J.; Kovnir, K. Unconventional Clathrates with Transition Metal-Phosphorus Frameworks. *Acc. Chem. Res.* **2018,** *51,* 31-39.

10. Dolyniuk, J.; Wang, J.; Lee, K.; Kovnir, K. Twisted Kelvin cells and truncated octahedral cages in the crystal structures of unconventional clathrates, AM_2P_4 (A = Sr, Ba; M = Cu, Ni) *Chem. Mater.* **2015,** *27,* 4476-4484.

11. Dolyniuk, J.; Zaikina, J.V.; Kaseman, D.C.; Sen, S.; Kovnir, K. Breaking the Tetra-Coordinated Framework Rule: New Clathrate $Ba_8M_{24}P_{28+\delta}$ (M = Cu/Zn). *Angew. Chem. Int. Ed.* **2017,** *56,* 2418-2422.

12. Dolyniuk, J.; Whitfield, P.S.; Lee, K.; Lebedev, O.I.; Kovnir, K. Controlling Superstructural Ordering in the Clathrate-I $Ba_8Cu_{16}P_{30}$ (M= Cu, Zn) through the Formation of Metal-Metal Bonds. *Chem. Sci.* **2017,** *8,* 3650-3659.

13. Perdew, J.P.; Burke, K.; Ernzerhof, M. Generalized Gradient Approximation Made Simple. *Phys. Rev. Lett.* **1997,** *77,* 3865-3868.

14. Clark, S. J.; Segall, M. D.; Pickard, C. J.; Hasnip, P. J.; Probert, M. J.; Refson, K.; Payne, M. C., First Principles Methods Using CASTEP. *Z. Kristallogr.* **2005,** *220,* 567-570.

15. Ramirez-Cuesta, A. J., aCLIMAX 4.0.1, The New Version of the Software for Analyzing and Interpreting INS Spectra. *Comp. Phys. Commun.* **2004**, *157*, 226-238.

16. Bruker APEX2; Bruker AXS Inc.: Madison, WI, 2005.

17. Sheldrick, G.M. A short history of SHELX. *Acta Crystallogr. Sect. A.* 2008, **A64**, 112-122.

18. Petricek, V.; Dusek, M.; Palatinus, L. Crystallographic Computing System JANA2006: General features. *Z. Kristallogr.* **2014,** *229,* 345-352.

19. Wang, J.; Lebedev, O.I.; Lee, K.; Dolyniuk, J.; Klavins, P.; Bux, S.; Kovnir, K. A high-efficiency thermoelectric $Ba_8Cu_{14}Ge_6P_{26}$: Bridging the gap between tetrel-based and tetrel-free clathrates. *Chem. Sci.* **2017,** *8,* 8030-8038.

20. Bhattacharya, A.; Carbogno, C.; Böhme, B.; Baitinger, M.; Grin, Yu.; Scheffler, M. Formation of Vacancies in Si- and Ge-based Clathrates: Role of Electron Localization and Symmetry Breaking. *Phys. Rev. Lett.* **2017,** *118,* 236401.

21. Shatruk, M. M.; Kovnir, K.; Shevelkov, A. V.; Presniakov, I. A.; Popovkin, B. A. First Tin Pnictide Halides $Sn_{24}P_{19.3}I_8$ and $Sn_{24}As_{19.3}I_8$: Synthesis and the Clathrate-I Type of the Crystal Structure. *Inorg. Chem.* **1999,** *38,* 3455-3457.

22. Zaikina, J. V.; Kovnir, K.; Sobolev, A. V.; Presniakov, I. A.; Prots, Yu.; Baitinger, M.; Schnelle, W.; Olenev, A. V.; Lebedev, O. I.; Van Tendeloo, G.; Grin, Yu.; Shevelkov, A. V. $Sn_{20.5}\square_{3.5}As_{22}I_8$: a largely disordered cationic clathrate with a new type of superstructure and abnormally low thermal conductivity. *Chem. Europ. J.* **2007,** *13,* 5090-5099.

23. Zaikina, J. V.; Schnelle, W.; Kovnir, K.; Olenev, A. V.; Grin, Yu.; Shevelkov, A. V. Crystal structure, thermoelectric and magnetic properties of the type-I clathrate solid solutions $Sn_{24}P_{19.3(2)}Br_xI_{8-x}$ ($0 \le x \le 8$) and $Sn_{24}P_{19.3(2)}Cl_yI_{8-y}$ ($y \le 0.8$). *Solid State Sciences,* **2007,** *9,* 664-671.

24. Wang, J.; Kaseman, D.; Lee, K.; Sen, S.; Kovnir, K. Enclathration of X@La_4 tetrahedra in channels of Zn-P frameworks in $La_3Zn_4P_6X$ (X = Cl, Br). *Chem. Mater.* **2016,** *28,* 4741-4750.

25. Sirusi, A. A.; Ross, J. H. Jr. Chapter Three - Recent NMR Studies of Thermoelectric Materials. *Ann. Re. NMR Spectr.* **2017,** *92,* 137-198.

26. Chen, J.-H.; Sirusi, A. A.; Zheng, X; Rodriguez, S.Y.; Ross, J. H. Jr. NMR and computational study of $Ba_8Cu_xGe_{46-x}$ clathrate semiconductors. *J. Alloys Comp.* **2014,** *593,* 261-266.

27. Fulmer, J.; Lebedev, O.I.; Roddatis, V.V.; Kaseman, D.; Sen, S.; Dolyniuk, J.; Lee, K.; Olenev, A.V.; Kovnir, K. Clathrate $Ba_8Au_{16}P_{30}$: The "Gold Standard" for Lattice Thermal Conductivity. *J. Amer. Chem. Soc.* **2013,** *135,* 12313-12323.

28. Kovnir, K.; Stockert, U.; Budnyk, S.; Prots, Yu.; Baitinger, M.; Paschen, S.; Shevelkov, A. V.; Grin, Yu. Introducing a Magnetic Guest to a Tetrel-Free Clathrate: Synthesis, Structure, and Properties of $Eu_xBa_{8-x}Cu_{16}P_{30}$ ($0 \le x \le 1.5$). *Inorg. Chem.* **2011,** *50,* 10387-10396.

29. Dolyniuk, J.; Kaseman, D.; Sen, S.; Zhao, J.; Osterloh, F.E.; Kovnir, K. *mP*-BaP_3: A New Phase from an Old Binary System. *Chem. Europ. J.* **2014,** *20*, 10829-10837.

30. Fulmer, J.; Kaseman, D.; Dolyniuk, J.; Lee, K.; Sen, S.; Kovnir, K. $BaAu_2P_4$: Layered Zintl Polyphosphide with Infinite (P^-) Chains. *Inorg. Chem.* **2013,** *52,* 7061-7067.

31. Pöttgen, R.; Hönle, W.; von Schnering, H. G. Encyclopedia of Inorganic Chemistry, 2nd ed.; King, R. B., Ed.; Wiley: Chichester, U.K., **2005**; Vol. VIII, pp 4255-4308.

32. Von Schnering, H. G. Hönle, W. Chemistry and structural chemistry of phosphides and polyphosphides. *Chem. Rev*. **1988**, *88*, 243-273.

33. Shatruk, M. M.; Kovnir, K.; Shevelkov, A. V.; Popovkin, B. A. Ag_3SnP_7: A Polyphosphide with a Unique $_\infty^1(P_7)$ Chain and a Novel Ag_3Sn Heterocluster. *Angew. Chem. Int. Ed. Engl.* **2000,** *39,* 2508-2509.

34. Zaikina, J. V.; Kovnir, K.; Haarmann, F.; Schnelle, W.; Burkhardt, U.; Borrmann, H.; Schwarz, U.; Grin, Yu.; Shevelkov, A. V. $Si_{172-x}P_xTe_y$ ($x = 2y$, $y > 20$) - The First Silicon-Based Cationic Clathrate III with High Thermal Stability. *Chem. Europ. J.* **2008,** *14*, 5414-5422.

35. Zaikina, J. V.; Kovnir, K.; Burkhardt, U.; Schnelle, W.; Haarmann, F.; Schwarz, U.; Grin, Yu.; Shevelkov, A. V. Cationic Clathrate I $Si_{46-x}P_xTe_y$ ($6.6(1) \leq y \leq 7.5(1)$, $x \leq 2y$): Crystal Structure, Homogeneity Range, and Physical Properties. *Inorg. Chem.* **2009,** *48,* 3720-3730.

36. Larsson, E. An X-ray investigation of the Ni-P system and the crystal structures of NiP and NiP_2. *Arkiv Kem.* **1965,** *23,* 335-365.

37. Ono, S.; Nomura, K.; Hayakawa, H. Syntheses of new rare-earth phosphides. *J. Less-Comm. Met.* **1974,** *38,* 119-130.

38. Huber, M.; Deiseroth, H.J. Crystal structure of zirconium diphosphide, ZrP_2. *Z. Kristallogr.* **1994,** *209,* 370-370.

39. Wang, J.; Lee, K.; Kovnir, K. Distorted phosphorus and copper square-planar layers in $LaCu_{1+x}P_2$ and $LaCu_4P_3$: synthesis, crystal structure, and physical properties. *Inorg. Chem.* **2015,** *54,* 890-897.

40. Aydemir, U.; Candolfi, C.; Borrmann, H.; Baitinger, M.; Ormeci, A.; Carrillo-Cabrera, W.; Chubilleau, C.; Lenoir, B.; Dauscher, A.; Oeschler, N.; Steglich, F.; Grin, Yu. Crystal structure and transport properties of $Ba_8Ge_{43}\square_3$. *Dalton Trans.* **2010,** *39,* 1078-1088.

41. Bandosz, T.J.; Seredych, M.; Rodriguez-Castellon, E.; Cheng, Y.Q.; Daemen, L.L.; Ramirez-Cuesta A.J., Evidence for CO_2 Reactive Adsorption on Nanoporous S- and N- Doped Carbon at Ambient Conditions. *Carbon* **2016**, *96*, 856-863.

42. Casco, M.E.; Cheng, Y.Q.; Daemen, L.L.; Fairen-Jimenez, D.; Ramos Fernandez, E.V.; Ramirez-Cuesta, A.J.; Silvestre-Albero, J., Gate-Opening Effect in ZIF-8: First Experimental Proof Using Inelastic Neutron Scattering. *Chem. Commun.* **2016**, *2*, 3639-3642.

43. Dong, J.; Sankey, O.F.; Myles, C.W., Theoretical Study of the Lattice Thermal Conductivity in Ge Framework Semiconductors. *Phys. Rev. Lett.* **2001**, *86*, 2361-2364.

44. Li, C.W.; Hong, J.; May, A.F.; Bansal, D.; Chi, S.; Hong, T.; Ehlers, G.; Delaire, O., Orbitally Driven Giant Phonon Anharmonicity in SnSe. *Nature Phys.* **2015**, *11*, 1063-1069.

45. Christensen, M.; Abrahamsen, A. B.; Christensen, N. B.; Juranyi, F.; Andersen, N. H.; Lefmann, K.; Andreasson, J.; Bahl, C. R. H.; Iversen, B. B. Avoided crossing of rattler modes in thermoelectric materials. *Nature Mater.* **2008,** *7,* 811-815.

46. Christensen, M.; Lock, N.; Overgaard, J.; Iversen, B. B. Crystal Structures of Thermoelectric n- and p-type $Ba_8Ga_{16}Ge_{30}$ Studied by Single Crystal, Multitemperature, Neutron Diffraction, Conventional X-ray Diffraction and Resonant Synchrotron X-ray Diffraction. *J. Amer. Chem. Soc.* **2006,** *128*, 15657-15665.

47. Christensen, S.; Schmøkel, M. S.; Borup, K. A.; Madsen, G. K. h.; McIntyre, G. J.; Capelli, S. C.; Christensen, M.; Iversen, B. B. “Glass-like” thermal conductivity gradually induced in thermoelectric $Sr_8Ga_{16}Ge_{30}$ clathrate by off-centered guest atoms. *J. Appl. Phys.* **2016,** *119,* 185102.

48. Hermann, R. P.; Keppens, V.; Bonville, P.; Nolas, G. S.; Grandjean, F.; Long, G. J.; Christen, H. M.; Chakoumakos, B. C.; Sales, B. C.; Mandrus, D. Direct Experimental Evidence for Atomic Tunneling of Europium in Crystalline $Eu_8Ga_{16}Ge_{30}$. *Phys. Rev. Lett.* **2006,** *97,* 017401.

49. Chakoumakos, B. C.; Sales, B. C.; Mandrus, D. G.; Nolas, G. S. Structural disorder and thermal conductivity of the semiconducting clathrate $Sr_8Ga_{16}Ge_{30}$. *J. Alloys Comp.* **2000,** *296,* 80-86.